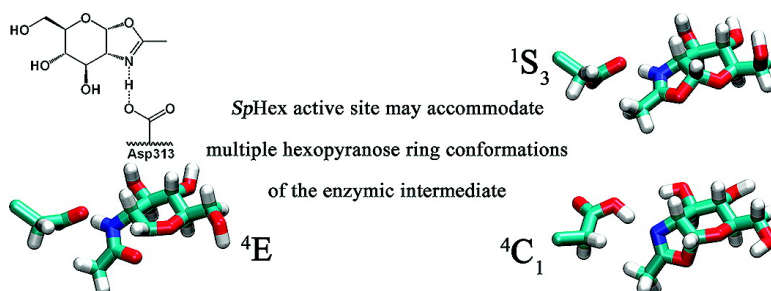Article

Elucidating the Nature of the *Streptomyces plicatus* #-Hexosaminidase-Bound Intermediate Using ab initio Molecular Dynamics Simulations

Ian R. Greig, Federico Zahariev, and Stephen G. Withers

*Sp*Hex active site may accommodate multiple hexopyranose ring conformations of the enzymic intermediate

More About This Article

Additional resources and features associated with this article are available within the HTML version:

- Supporting Information
- Access to high resolution figures
- Links to articles and content related to this article
- Copyright permission to reproduce figures and/or text from this article

View the Full Text HTML

ACS Publications
High quality. High impact.

Elucidating the Nature of the *Streptomyces plicatus* β-Hexosaminidase-Bound Intermediate Using ab initio Molecular Dynamics Simulations

Ian R. Greig,[†] Federico Zahariev, and Stephen G. Withers*

Department of Chemistry, University of British Columbia, Vancouver, Canada V6T 1Z3

Received July 19, 2008; E-mail: withers@chem.ubc.ca

Abstract: By using all-atom ab initio molecular dynamics simulations, the solution pK_a of the oxazolinium ion intermediate formed during the *Streptomyces plicatus* β-hexosaminidase (*Sp*Hex)-catalyzed hydrolysis of β-D-*N*-acetylglucosaminides is estimated as $pK_a = 7.7$. The structure and protonation state of the enzyme-bound intermediate have also been investigated, using hybrid QM/MM methods. The protonation state and conformational properties of the enzyme bound intermediate are found to be sensitive to the protonation state of a number of ionisable residues (other than the aspartate−glutamate catalytic dyad) suggesting that the microscopic electrostatic environment of *Sp*Hex not only perturbs the relative magnitudes of the pK_a values of the Asp side chain carboxylate and oxazolinium ion but also that *Sp*Hex binds its intermediate in a distorted conformation with respect to its ground-state conformation in solution.

Introduction

The majority of enzymes catalyzing the hydrolysis of glycosides with retention of stereochemistry at the anomeric center utilize a double-displacement mechanism requiring the presence of two amino acids whose side chains bear carboxylic acid or carboxylate groups. Subtle variations on this mechanism are found in the case of sialidases and trans-sialidases (which utilize tyrosine as the enzymic nucleophile),[1,2] and glycoside hydrolases belonging to CAZY families 18 (chitinases), 20 (hexosaminidases), 56 (hyaluronidases), 84 (*O*-GlcNAcases), and 85 (endo-β-*N*-glucosaminidases).[3−6] These latter families of glycoside hydrolases utilize a common mechanism for the hydrolysis of *N*-acetylglucosamine- and *N*-acetylgalactosamine-containing oligosaccharides and glycoconjugates (http://www-.cazy.org)[7] in which the *N*-acetamido group of the substrate acts as an intramolecular nucleophile (neighboring group assistance) to displace the leaving group aglycone (Figure 1). [A more dramatic variation in the mechanism of glycoside hydrolysis is seen in the case of GH-4 and GH-109 enzymes which employ mechanisms involving redox chemistry.[8]]

The catalytic activities of members of these glycoside hydrolase (GH) families have been associated with a number of disease states in mammals including asthma (GH-18),[9] Tay-Sachs and Sandhoffs diseases (GH-20),[10,11] male infertility disorder (GH-56),[12] and Alzheimer's (GH-84).[13] A greater understanding of the mechanism of action of these families of enzymes may ultimately facilitate the development of transition state-based inhibitors as therapeutic agents.

Although the mechanism of glycoside hydrolysis employed by these enzymes does not require the presence of an enzymic nucleophile, it has been found that two carboxylic acid-bearing residues are still required for optimal catalytic activity. In the case of GH-20 and GH-84 enzymes, these residues are adjacent in the primary sequence whereas, in the case of GH-18, GH-56, and GH-85 enzymes, they are separated by one other residue. In the case of the GH-20 enzyme *Streptomyces plicatus* β-hexosaminidase (*Sp*Hex), two carboxylic residues have been identified as being critical to the catalytic function of the enzyme. Glutamic acid 314 acts as a general acid, facilitating glycoside bond cleavage through protonation of the oxygen atom of the departing aglycon moiety. Aspartate 313 is located adjacent to the amide nitrogen, but its precise role is less clear. Kinetic studies suggest it is deprotonated in its catalytically active form, and structural studies have shown that it optimally

[†] Current address: Department of Chemistry, University of Bath, Bath BA2 7AY, U.K.

(1) Watson, J. N.; Dookhun, V.; Brogford, T. J.; Bennet, A. J. *Biochemistry* **2003**, *42*, 12682–12690.

(2) Watts, A. G.; Damager, I.; Amaya, M. L.; Buschiazzo, A.; Alzari, P.; Frasch, A. C.; Withers, S. G. *J. Am. Chem. Soc.* **2003**, *125*, 7532–7533.

(3) Tews, I.; Perrakis, A.; Oppenheim, A.; Dauter, Z.; Wilson, K. S.; Vorgias, C. E. *Nat. Struct. Mol. Biol.* **1996**, *3*, 638–648.

(4) Chao, K. L.; Muthukumar, L.; Herzberg, O. *Biochemistry* **2007**, *46*, 6911–6920.

(5) Vocadlo, D. J.; Withers, S. G. *Biochemistry* **2005**, *44*, 12809–12818.

(6) Macauley, M. S.; Whitworth, G. E.; Debowski, A. W.; Chin, D.; Vocadlo, D. J. *J. Biol. Chem.* **2005**, *280*, 25313–25322.

(7) Coutinho, P. M.; Henrissat, B. Carbohydrate-active enzymes: an intergrated database approach. In *Recent Advances in Carbohydrate Bioengineering*; Gilbert, H. J., Davies, G., Henrissat, B., Svensson, B., Eds.; The Royal Society of Chemistry: Cambridge, U.K., 1999; pp 3−12.

(8) Yip, V. L. Y.; Varrot, A.; Davies, G. J.; Rajan, S. S.; Yang, X.; Thompson, J.; Anderson, W. F.; Withers, S. G. *J. Am. Chem. Soc.* **2004**, *126*, 8354–8355.

(9) Reese, T. A.; Liang, H.-E.; Tager, A. M.; Luster, A. D.; Van Rooijen, N.; Voehringer, D.; Locksley, R. M. *Nature* **2007**, *447*, 92–97.

(10) Mark, B. L.; Mahuran, D. J.; Cherney, M. M.; Zhao, D.; Knapp, S.; James, M. N. *J. Mol. Biol.* **2003**, *327*, 1093–1109.

(11) Lemieux, M. J.; Mark, B. L.; Cherney, M. M.; Withers, S. G.; Mahuran, D. J.; James, M. N. *J. Mol. Biol.* **2006**, *359*, 913–929.

(12) Abdul-Aziz, M.; Meriano, J.; Casper, R. F. *Fertility Sterility* **1996**, *65*, 977–980.

(13) Liu, F.; Iqbal, K.; Grundke-Iqbal, I.; Hart, G. W.; Gong, C. X. *Proc. Natl. Acad. Sci. U.S.A.* **2004**, *101*, 10804–10809.
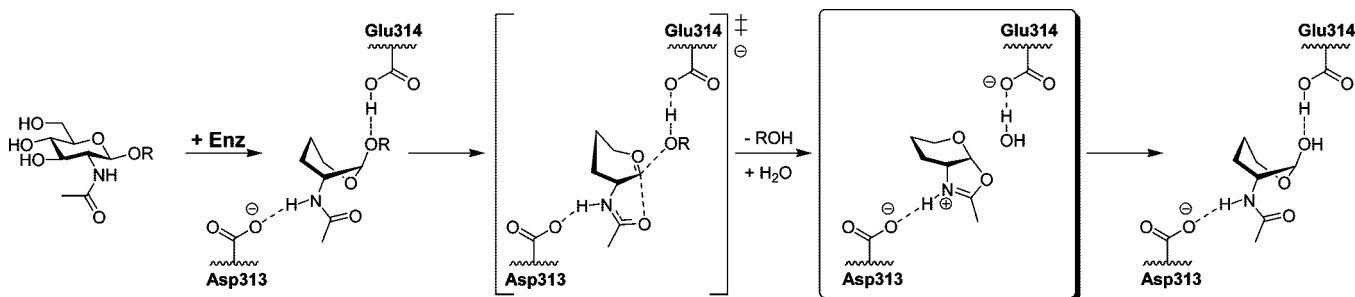
Figure 1. *Streptomyces plicatus* β-hexosaminidase hydrolyses β-configured glycosides with retention of stereochemistry at the anomeric center. Kinetic studies have implicated the role of the substrate 2-*N*-acetamido group as the catalytic nucleophile (anchimeric assistance) in a mechanism utilizing neighboring group participation.[5] The current QM/MM study (vide infra) characterizes the enzyme-bound intermediate highlighted.

orients the *N*-acetamido group of the substrate for nucleophilic attack at the anomeric center.[14]

A dramatic decrease in the pK_a of the substrate's *N*-acetamido group is predicted as the amide group found in the substrate (pK_a > 15) is converted to the oxazolinium ion of the intermediate (the pK_a of the model compound 2-methyl-Δ^2-oxazolinium ion **1** is 5.5).[15] Asp313 may therefore fulfill one of two catalytic roles: if the pK_a of the enzyme-bound intermediate falls below that of Asp313, then the libido rule predicts that, as proton transfer from oxazolinium ion to Asp313 is thermodynamically favorable in the intermediate state, then coupling of proton transfer and heavy atom rearrangement at the transition state may occur at the transition state (i.e., Asp313 acts as a general base catalyst); alternatively, if the pK_a of the enzyme-bound intermediate remains above that of Asp313, then proton transfer cannot occur in either the intermediate state or the preceding transition state and the role of Asp313 is limited to that of orienting and polarizing the *N*-acetamido group and electrostatically stabilizing the incipient oxazolinium ion intermediate.[16,17]

Prior molecular mechanics MD studies of *Serratia marcescens* Chitinase A and hevamine (both members of GH-18) have implicated the importance of substrate distortion in the Michaelis complex[18] and of anchimeric assistance in the mechanism.[19] The MM potentials used in these modeling studies did not permit consideration of the multiple possible protonation states of the enzyme-bound intermediate within a wider enzyme environment (and hence the alternative catalytic roles of the second conserved catalytic carboxylate group). In this paper, we describe an ab initio MD-based prediction of the pK_a of oxazolinium ion **2** free in solution and QM/MM MD simulations of the enzyme-bound oxazolinium ion aimed at elucidating the catalytic role of Asp313 and the nature of the enzyme-bound intermediate.
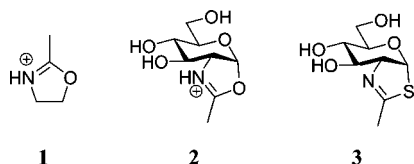
Methods

All simulations of systems involving QM atoms were performed in the CPMD program using the BLYP gradient-corrected exchange-correlation functional to treat quantum mechanical atoms.[20] The core electrons were treated using nonlocal, norm-conserving Troullier-Martins pseudopotentials, transformed according to the Kleinman−Bylander scheme. The wave functions of the valence electrons were treated with an energy cutoff of 70 Ry in a plane wave basis set. QM/MM simulations were performed using the CPMD/GROMOS96 code of Röthlisberger et al.[21] The equations of motion were integrated using a time-step of 4.0 atomic units (au). A fictitious electronic mass of 400 au was used. Preliminary simulations involving only MM atoms were conducted using the GROMOS96 suite of MD programs.[22]

Aqueous Simulation. Molecular mechanics MD simulations at constant temperature (300 K) were conducted on constant size cubic boxes containing oxazolinium ion **2** ($^4C_1$ conformation) and a number of water molecules treated using the SPC/E model. An ad hoc topology was used for the oxazolinium ion based on the carbohydrate parameters of Hünenberger.[23] Simulations consisting of 1 ns equilibration and 1 ps of production dynamics were performed. The box size and number of water molecules were adjusted until the average pressure exerted by the periodic box over the course of the production run reproduced atmospheric pressure. Radial distribution functions for water atoms ($O_{water}O_{water}$, $H_{water}O_{water}$, and $H_{water}H_{water}$) were calculated to verify that there was no significant deviation from their bulk values (data not shown).

The oxazolinium ion **2** (Figure 2), solvated by 69 water molecules in a periodically repeating cubic cell of side length, $L = 14.05$ Å, was subjected to a series of short, consecutive all-atom QM MD trajectories during which the ionic temperature was controlled by rescaling (300 K) and the wave function regularly reoptimized to equilibrate the system.

Production dynamics were conducted using a Nosé−Hoover thermostat (target temperature 300 K, frequency 3000 cm^{-1}, chain length 4) to control the ionic temperature. Unconstrained dynamics were conducted for 10 ps prior to the introduction of a distance-based restraint on the N−H distance. The N−H distance was increased in steps of 0.05 Å, and MD trajectories involving 1 ps equilibration and 3−6 ps production dynamics were generated to produce well converged mean constraining forces. Over the course of the production trajectory, the force needed to restrain the N−H distance to its target length was recorded. A potential of mean force for controlled dissociation of the weak acid was constructed and used to estimate a pK_a value following Sprik's treatment of weak

(14) Williams, S. J.; Mark, B. L.; Vocadlo, D. J.; James, M. N.; Withers, S. G. *J. Biol. Chem.* **2002**, *277*, 40055–40065.
(15) Porter, G. R.; Rydon, H. N.; Schofield, J. A. *Nature* **1958**, *182*, 927.
(16) Jencks, W. P. *J. Am. Chem. Soc.* **1972**, *94*, 4731–4732.
(17) Jencks, W. P. *Chem. Rev.* **1972**, *72*, 705–718.
(18) Brameld, K. A.; Goddard, W. A., III *J. Am. Chem. Soc.* **1998**, *120*, 3571–3590.
(19) Brameld, K. A.; Schrader, W. D.; Imperiali, B.; Goddard, W. A., III *J. Mol. Biol.* **1998**, *280*, 913–923.
(20) Car, R.; Parrinello, M. *Phys. Rev. Lett.* **1985**, *55*, 2471–2474.
(21) Laio, A.; VandeVondele, J.; Röthlisberger, U. *J. Chem. Phys.* **2002**, *11*, 6941–6948.
(22) Scott, W. R. P.; Hünenberger, P. H.; Tironi, I. G.; Mark, A. E.; Billeter, S. R.; Fenner, J.; Torda, A. E.; Krueger, P.; van Gunsteren, W. F. *J. Phys. Chem. A* **1999**, *103*, 3596–3607.
(23) Lins, R. D.; Hünenberger, P. H. *J. Comput. Chem.* **2005**, *26*, 1400–1412.
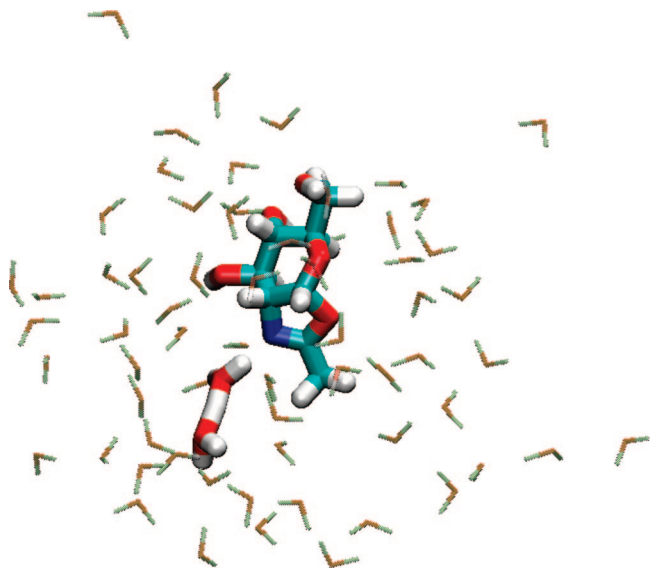
Figure 2. In the QM MD simulations of oxazolinium ion **2** deprotonation, the oxazolinium ion is solvated by 69 water molecules. This snapshot is taken from a trajectory associated with a large value of the constrained distance, *r*. Proton transfer to the coordinating water molecule is complete, and the excess proton is shared between the water molecule that effects deprotonation and a second coordinating water molecule to form a Zundel ($H_5O_2^+$) ion.

acid dissociation,[24,25] which uses Chandler's statistical mechanical method of treating dissociation reactions.[26] Briefly, the fraction of HA molecules dissociated, $\alpha(R_c)$, when H and A are separated by some distance R_c is given by

$$\alpha(R_c) = 1 - \frac{\int_0^{R_c} 4\pi r^2 \exp[-\Delta w(r)/k_B T]}{\int_0^{R_{max}} 4\pi r^2 \exp[-\Delta w(r)/k_B T]}$$

where $\Delta w(r)$ is the change in potential of the mean force. The dissociation fraction is in turn used to estimate the equilibrium constant, K_a, by

$$K_a = \left(\frac{\alpha(R_c)^2}{1 - \alpha(R_c)}\right)\frac{N}{c_0 V}$$

where N is the number of HA molecules in the simulation cell (=1), V is the size of the simulation cell used, and c_0 is the standard concentration.

Enzymic Simulation. The X-ray crystal structure of *Sp*Hex bound to thiazoline **3** (a nonhydrolyzable oxazolinium ion intermediate-analogue) determined at 2.10 Å resolution was used as the starting point for MD simulations (PDB accession code 1HP5).[27] The protonation states of the two critical catalytic groups Asp313 and Glu314 were assigned to be those required by a catalytically competent enzyme-intermediate complex. Glu314 acts as a base catalyst in the second step of the enzymic reaction (oxazolinium ion hydrolysis), enhancing the reactivity of a suitably positioned water molecule: it is therefore present in its deprotonated form; Asp313 is assumed to be present in its deprotonated form as it acts as a hydrogen bond acceptor from the oxazolinium ion intermediate. The influence of the protonation states of a number of other ionisable residues (Asp395 and Glu444) found in the active site of

*Sp*Hex on the structure of bound intermediate was investigated in a series of separate MD simulations (see Results and Discussion).

The resulting proteins were solvated by approximately 14 000 water molecules in a 67.4 Å × 76.9 Å × 92.5 Å periodically repeating box. The systems were minimized, and net charge neutrality was enforced on the system by the replacement of noncrystallographic water molecules by chloride ions. MM MD simulations were carried out using periodic boundary conditions in the NPT ensemble at atmospheric pressure and 300 K (Berendsen baths). The initial temperature of the system was 300 K with atomic velocities taken from a Maxwellian distribution. A time step of 2 fs was used to integrate the equations of motion with bond lengths constrained at their equilibrium values using the SHAKE algorithm. The system was allowed to equilibrate for 0.25 ns before a further 3 ns MD run carried out.

Snapshots from the MM simulations described above were used as starting points for the 10−12 ps, NVT QM/MM simulations of the enzyme-bound intermediate The electrostatic interaction of the quantum system with the MM system was explicitly taken into account for all MM atoms up to 12 au away from any QM atom. A cell size of 25.0 au × 20.0 au × 31.0 au was used for the QM atoms. The electrostatic interaction of the QM atoms with the remaining MM atoms was treated using a multipole expansion (up to quadrupoles) for the QM atoms. A monovalent carbon atom pseudopotential [Supplied by Ute Röhrig of the Röthlisberger group] was used to terminate the QM region at the backbone carbon atom of the Asp313 residue. QM and MM regions were equilibrated separately at 300 K using the CAFES method[28] before extended QM/MM simulations of the entire enzyme-bound intermediate were carried out under the control of a single Nosé−Hoover thermostat (300 K, 3000 cm⁻¹) for both QM and MM atoms.

Results and Discussion

Estimation of Oxazolinium Ion pK_a in Solution. The controlled deprotonation of acids during ab initio MD simulations using distance or coordination constraints has been shown to take place in three distinct phases: (1) at low constrained distance, the reaction coordinate corresponds to stretching of the H−A covalent bond; (2) proton transfer between H−A and the solvating (hydrogen bond acceptor) water molecule occurs; (3) diffusion of the solvent "bound" excess proton throughout the solution.[29] Progress from phase 1 to phase 2 is represented by a decrease in the distance separating the hydrogen-bonded heteroatoms (see Figure S1 of the Supporting Information).[30]

The potential of the mean force obtained for the deprotonation of oxazolinium ion **2** (Figure 3A) is unusual as at high values of the constrained distance although a gradual diminution in the mean constraining force is observed; this is followed by a slight increase in the PMF (i.e., the gradient of the mean constraining force never becomes negative). This unphysical behavior is likely due to the use of the BLYP functional in combination with a relatively small fictitious electron mass as the constraining forces determined were found to be well converged in our simulations. Our choice of a small fictitious electron mass (400 au) ensures that no significant deviations from the Born−Oppenheimer surface are likely to occur over the time-scale simulated;[31] however, the BLYP functional, in

(24) Doltsinis, N. L.; Sprik, M. *Phys. Chem. Chem. Phys.* **2003**, *5*, 2612–2618.
(25) Davies, J. E.; Doltsinis, N. L.; Kirby, A. J.; Roussev, C. D.; Sprik, M. *J. Am. Chem. Soc.* **2002**, *124*, 6594–6599.
(26) Chandler, D. *Introduction to Modern Statistical Mechanics*; Oxford University Press: New York, 1987.
(27) Mark, B. L.; Vocadlo, D. J.; Knapp, S.; Triggs-Raine, B. L.; Withers, S. G.; James, M. N. *J. Biol. Chem.* **2001**, *276*, 10330–10337.
(28) VandeVondele, J.; Röthlisberger, U. *J. Phys. Chem. B* **2002**, *106*, 203–208.
(29) Ivanov, I.; Klein, M. L. *J. Am. Chem. Soc.* **2002**, *124*, 13380–13381.
(30) Ivanov, I.; Chen, B.; Raugei, S.; Klein, M. L. *J. Phys. Chem. B* **2006**, *2006*, 6365–6371.
(31) Grossman, J. C.; Schwegler, E.; Draeger, E. W.; Gygi, F.; Galli, G. *J. Chem. Phys.* **2004**, *120*, 300–311.
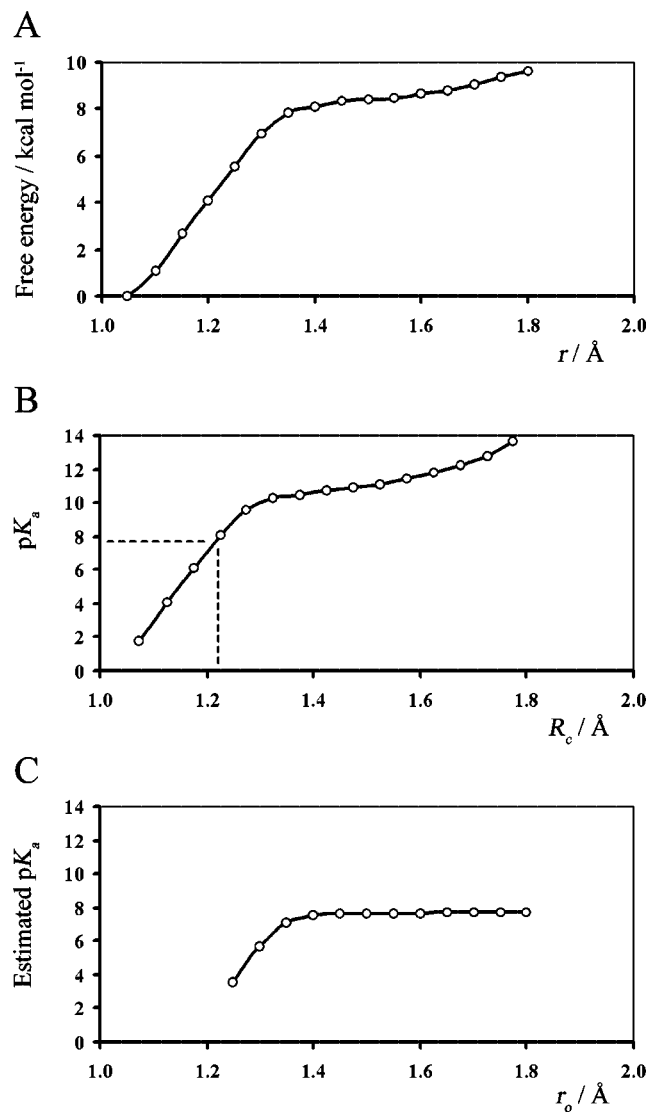
A

B

C

Figure 3. (A) Potential of the mean force determined for deprotonation of oxazolinium ion **2** using a single distance constraint. (B) The pK_a of oxazolinium ion **2** is determined using the value of cutoff distance, $R_c = 1.22$ Å determined by Sprik. [25] (C) The reduced rates of excess proton diffusion at high values of constrained distance r, arising from the use of the BLYP functional, do not significantly influence the estimated pK_a value (see text).

combination with small fictitious electron masses, has been shown to produce unphysical behavior by Voth.[32] Not only does this combination of functional and simulation parameter tend to underestimate proton diffusion rates (resulting in an over-structured water environment) in CPMD simulations of the excess proton in water, but more intriguingly, over extended simulations, the excess proton is found to be preferentially associated with a particular oxygen atom. The existence of such so-called "special" water oxygen atoms in a time averaged sense is consistent with the presence of a restoring force on the proton toward the oxazoline nitrogen atom in our simulation. In spite of the shortcomings of the BLYP functional in treating the behavior of the excess abstracted proton at high constrained distances, we show that these pathologies do not significantly affect the pK_a value estimated for the oxazolinium ion **2** (vide infra).

(32) Izvekov, S.; Voth, G. A. *J. Chem. Phys.* **2005**, *123*, 044505.

The estimation of the pK_a values of weak acids from PMF data according to statistical mechanical principles[26] is critically dependent on the cutoff radius chosen to specify at which point the bond between the HA dimer is determined to have been formed ($r < R_c$).[24] The most rigorous approach adopted to date is that of Ivanov and Klein in examining histidine deprotonation.[30] Their simulations utilized highly converged trajectories and represented the limit in accuracy that can be obtained with respect to the chosen functional and (single) reaction coordinate used. They found that a number of structural and electronic properties of the molecular dynamics trajectories generated at different distance constraints could be used to produce a highly converged value for the pK_a of histidine, relative to that of water.[30] Subsequent notable work on weak acid deprotonation in the condensed phase has focused on the use of multiple collective variables in describing the deprotonation process using metadynamics simulations.[33] We adopt the simpler approach of Sprik in treating R_c as an adjustable parameter.[25] A value of $R_c = 1.22$ Å was found to reproduce the experimentally determined dissociation constant of water when the BLYP functional was used.[34,35] The variation of estimated pK_a value with R_c, derived from the PMF of Figure 3A, is shown in Figure 3B. At a value of $R_c = 1.22$ Å, the estimated pK_a of oxazolinium ion **2** is 7.7. [Klein and Ivanov (ref 30) have shown that converged, accurate relative pK_a values of water and histidine may be obtained for any cutoff radii in excess of around 1.15 Å. They find that the choice of similar cutoff radii for both water and histidine deprotonation is justified by the similarity of a number of electronic and structural parameters character-izing these deprotonations.]

The upward tail of the PMF does not significantly influence the value of pK_a estimated. This may be demonstrated by (arbitrarily) setting components of the mean constraining forces for radii, $r > r_0$, to zero and recalculating the estimated pK_a (using $R_c = 1.22$ Å throughout). As can be seen from Figure 3C, the estimated pK_a is not significantly influenced by systematic errors arising from deficiencies of the BLYP functional when used with low fictitious electron masses: for values of r_0 greater than or equal to 1.35 Å, the estimated pK_a value varies by less than 0.6 pK_a units, and for r_0 greater than or equal to 1.40 Å, this variation is by less than 0.1 pK_a units. During proton transfer processes, the distance separating het-eroatoms is found to contract up to the point that the reactive event occurs, diffusion of the excess proton throughout the solution is unimportant prior to this event. We find that the minimum in the average distance separating the oxazolinium nitrogen and coordinating water oxygen atoms occurs at around 1.40 Å. Since errors arising due to use of the BLYP functional cannot be significant prior to the completion of proton transfer (i.e., $r < 1.35-1.40$ Å) and errors arising in the estimated pK_a value due to this deficiency are insignificant for gradients above 1.35 Å, the determination of a molecule's pK_a is not critically dependent on the accurate treatment of the proton's behavior at high constrained distances.

The theoretically determined pK_a value of oxazolinium ion **2** may be compared with a pK_a value of 5.5 measured for 2-methyl-Δ^2-oxazolinium ion **1**.[15] We suppose that perhaps the pK_a value of oxazolinium ion **2** is higher than that of **1** due to electronic factors. Contribution of the no-bond resonance

(33) Park, J. M.; Laio, A.; Iannuzzi, M.; Parrinello, M. *J. Am. Chem. Soc.* **2006**, *128*, 11318–11319.
(34) Trout, B. L.; Parrinello, M. *Chem. Phys. Lett.* **1998**, *288*, 343–347.
(35) Trout, B. L.; Parrinello, M. *J. Phys. Chem. B* **1999**, *103*, 7340–7345.

structure **4** (possessing a proton with an amide-like pK_a value) will tend to produce a higher pK_a value for oxazolinium ion **2** when compared to oxazolinium ion **1**, in which such considerations are absent. Our calculated pK_a value is consistent with the experimentally observed pH-dependent behavior of reactions in which oxazolinium ion **2** has been observed as an intermediate.[36]

2   **4**
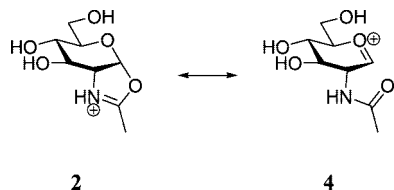
Structural Characterization of the *Sp*Hex-Bound Intermediate. The QM MD simulation of oxazolinium ion **2** in aqueous solution provides an estimate of its pK_a value, which is comparable to the pK_a of the side chain carboxylic acid of an aspartic acid residue in solution. The heterogeneous environment of the *Sp*Hex active site will however perturb the relative pK_a values of both Asp313 and the oxazolinium ion. The pK_a value tentatively assigned to Asp313 is that of the acidic limb of the pH-rate profile of *Sp*Hex and may not reliably reflect the true microscopic pK_a of Asp313. [Experimentally, the microscopic pK_a value of a particular residue may in principle be assigned by examination of changes in ^{13}C NMR chemical shifts with changing solution pH, but such data is not available for *Sp*Hex.[37] Theoretical estimates of the microscopic pK_a values of *Sp*Hex's titratable residues do suggest that the kinetically determined pK_a of Asp 313 approximately corresponds to its microscopic pK_a.[38,39]] With these reservations in mind, it is desirable to probe the interaction of Asp313 with the enzyme-bound intermediate using a QM treatment of Asp313 and the oxazolinium ion within a QM/MM framework in which the remaining protein and solvent residues are treated using an MM framework. The QM treatment of Asp313 and the bound intermediate affords the possibility of proton transfer occurring between the heteroatom centers of Asp313 and the oxazolinium ion; the QM/MM coupling scheme accounts for the perturbation of the relative, microscopic pK_a values of Asp313 and oxazolinium ion through electrostatic interactions with the environment. Furthermore, the QM treatment of the enzyme-bound intermediate will afford a better description of the conformational properties of the intermediate than the ad hoc topology used in the preliminary MM simulations.[40]

The experimentally determined pH-rate (k_{cat}/K_m) profile of wild-type *Sp*Hex is consistent with activity arising predominantly due to the ionization states of the two catalytic residues. A broad shoulder in the pH-rate profile was however observed at high pH values suggesting that multiple enzyme protonation states contribute to the observed rates of reaction. The states likely arise from the ionization of residues other than Asp313 and Glu314 within the active site of *Sp*Hex. This suggestion is supported by the pH-rate profile of the Asp313Ala mutant of

*Sp*Hex in which a bell-shape profile (albeit with reduced activity and shifted pH optimum) was again observed.[14] In light of these observations, the role that the protonation states of active site residues other than Asp313 and Glu314 play in determining the structure of the enzyme-bound intermediate was investigated.

Three residues possessing carboxylic acid-bearing side chains (other than Asp313 and Glu314) are found within the active site of *Sp*Hex (Asp191, Glu444, and Asp395). Of these three residues, Glu444 and Asp395 are found in the first solvation shell of *Sp*Hex-bound thiazoline **3** and make direct hydrogen-bonding contacts with the 6- and 4-hydroxyl groups of the ligand; the interaction between Asp191 and the 3-hydroxyl group of thiazoline **3** is mediated by a crystallographic water molecule (Figure 4). Theoretical estimations of the pK_a values associated with these three residues suggest that the pK_a of Asp191 will be dramatically depressed due to the proximity of positively charged histidine and arginine residues;[38] the pK_a values of Asp395 and Glu444 are predicted to be around those of the catalytic residues and hence the enzyme pH-rate optimum (see Table S1 of the Supporting Information). On the basis of these observations, MD simulations of four different protonation states for the Asp395−Glu444 residue pair were conducted. These simulations are identified as AspH395−GluH444, Asp395−GluH444, AspH395−Glu444, and Asp395−Glu444 according to whether both Asp395 and Glu444, just Asp395, just Glu444, or neither Asp395 nor Glu444 were protonated, respectively. The evolution of structural parameters observed during the QM/MM MD simulation of Asp395−Glu444 was found to closely mirror those of Asp395−GluH444, and so, only the results of the simulation of Asp395−GluH444 are presented.

The initial MM equilibration of the protein structures produced no discernible change in the overall fold. RMSD values based on the α-carbon atoms of the peptide backbone, calculated with respect to the crystallographically determined structure, of 1.7 Å (AspH395−GluH444), 1.6 Å (Asp395−GluH444), and 1.9 Å (AspH395−Glu444) were obtained. The snapshots chosen from the MM trajectories and utilized as starting points for the QM/MM MD simulations each contained broadly similar dispositions of residues within the enzyme active site (Figure 5). The only significant deviations in active-site structures observed between the crystallographically determined structure of *Sp*Hex-bound thiazoline **3** and the three simulated structures of the *Sp*Hex-bound oxazolinium ions **2** involved the loss of the crystallographic water molecule from the active site (OW, Figure 4C) and the insertion of a second water molecule forming a bridge between Asp395 (in either of its protonation states) and the 6-hydroxyl group of the ligand.

The evolution of a number of structural parameters was followed over the course of the QM/MM MD simulation as a means of characterizing the nature of the enzyme-bound intermediate: the N2−H2 and O$_{ASP}$−H2 bond distances (which characterize the heteroatom center that the proton is bonded to), the C$_{anomeric}$−O$_{oxazoline}$ and C$_{anomeric}$−O$_{pyranose}$ bond distances (indicative of whether any distortion from a stable enzyme-bound intermediate toward reactive, oxacarbenium ion-like species occurs), and the pyranose ring conformation (Figure 6). The last of these structural parameters was defined according to the method of Bércés et al. in which the redundant set of six internal pyranose ring dihedrals is used to specify a conformation in terms of a polar angle θ ($0° \leq \theta \leq 180°$), an equatorial angle

(36) Ballardie, F. W.; Capon, B.; Dearie, W. M.; Foster, R. L. *Carbohydr. Res.* **1976**, *49*, 79–92.

(37) McIntosh, L. P.; Hand, G.; Johnson, M. D.; Körner, M.; Plesniak, L. A.; Ziser, L.; Wakarchuk, W. W.; Withers, S. G. *Biochemistry* **1996**, *35*, 9958–9966.

(38) Li, H.; Robertson, A. D.; Jensen, J. H. *Proteins: Struct., Funct., Bioinf.* **2005**, *61*, 704–721.

(39) Kongsted, J.; Ryde, U.; Wydra, J.; Jensen, J. H. *Biochemistry* **2007**, *46*, 13581–13592.

(40) Biarnés, X.; Nieto, J.; Planas, A.; Rovira, C. *J. Biol. Chem.* **2006**, *281*, 1432–1441.
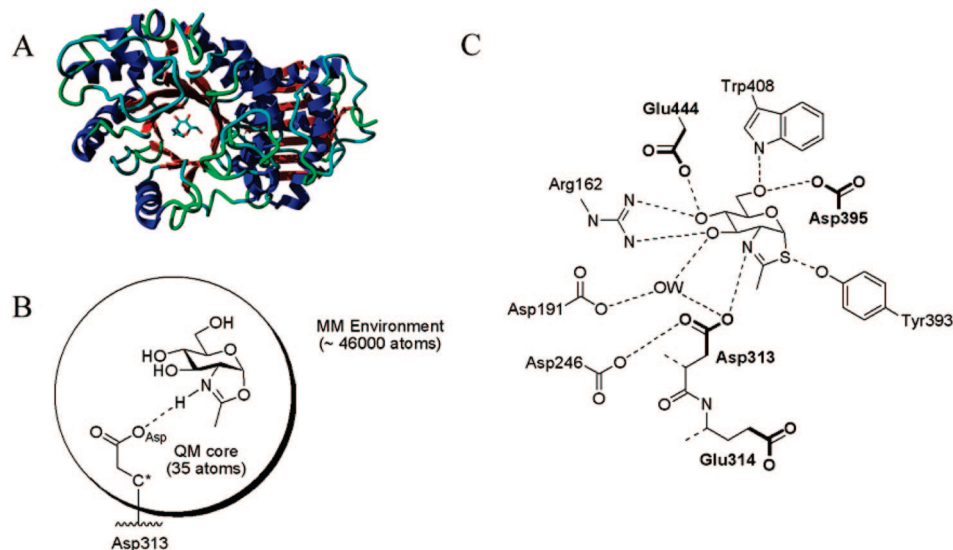
Figure 4. (A) The nonhydrolyzable intermediate analogue thiazoline **3** bound in the active site of *Sp*Hex (PDB 1HP5) was used as the starting point for MM and QM/MM MD simulations of oxazolinium ion **2**. (B) Oxazolinium ion **2** and part of Asp313 were treated using a QM Hamiltonian to allow proton transfer between enzyme-bound intermediate and catalytic residue. (C) Multiple hydrogen-bond donors and acceptors are found in contact with the enzyme-bound intermediate in the active site of *Sp*Hex. The protonation states of residues marked in bold are significant: Asp313 and Glu314 are deprotonated in the kinetically competent intermediate species (assuming that oxazolinium ion **2** is initially protonated in the active site); the influence of the protonation states of Asp395 and Glu444 on the structure of the enzyme-bound intermediate was investigated.
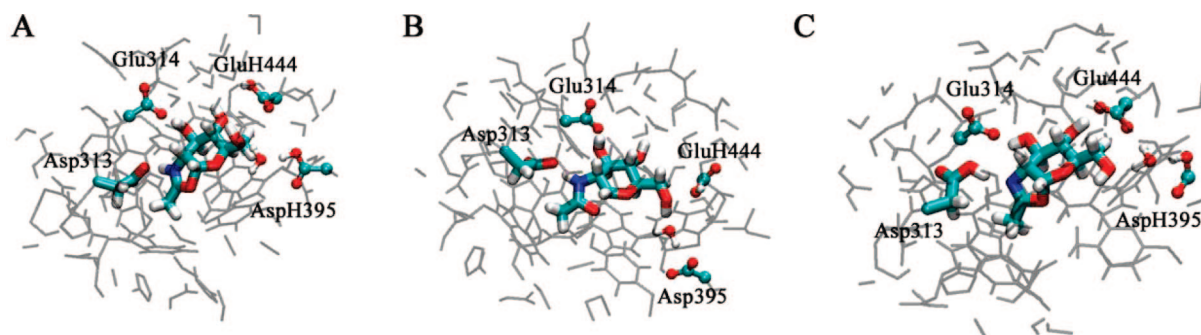

Figure 5. Snapshots taken from QM/MM MD simulations showing the typical disposition of residues with the *Sp*Hex active site. Panels A, B, and C refer to simulations of the different protonation states treated: AspH395−GluH444, Asp395−GluH444, and AspH395−Glu444, respectively.
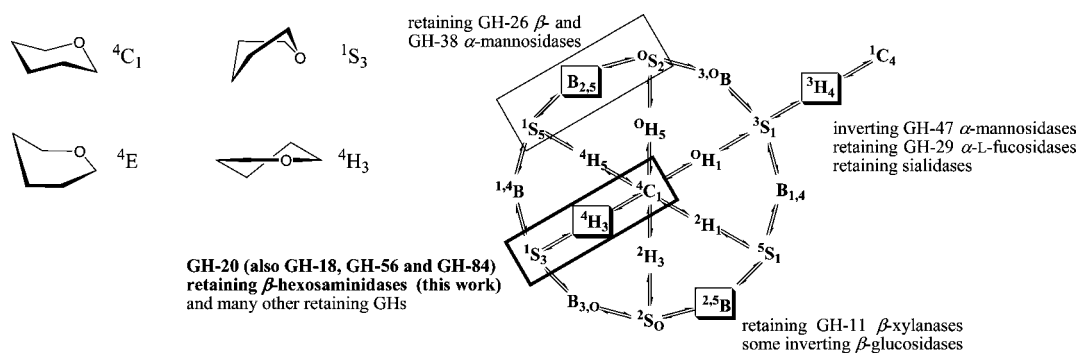

Figure 6. Representative hexopyranose ring conformations (top left) and conformational itineraries (right, adapted from ref 42) derived from crystallographically determined structures.

φ ($-180° \leq \varphi < +180°$), and an amplitude r.[41] Changes in the polar angle θ specify a $^1C_4$ chair ($\theta = 0°$), envelope/half-chair ($\theta = 45°$), boat/skew-boat ($\theta = 90°$), envelope/half-chair ($\theta = 135°$), and $^4C_1$ chair ($\theta = 180°$) transformation whereas changes in the equatorial angle φ specify a boat-skew-boat (for

$\theta = 90°$) or envelope-half-chair (for $\theta = 45°$ or $135°$) pseudorotational itinerary. Angles θ and φ are sufficient to specify which of the 38 canonical pyranose conformations a molecule is closest to; the amplitude r specifies the extent of puckering distortion from a planar six-membered ring.

Figure 7 shows the evolution of these characteristic distances during the course of the QM/MM MD simulation of the *Sp*Hex-bound intermediate. Structurally distinct behavior is observed

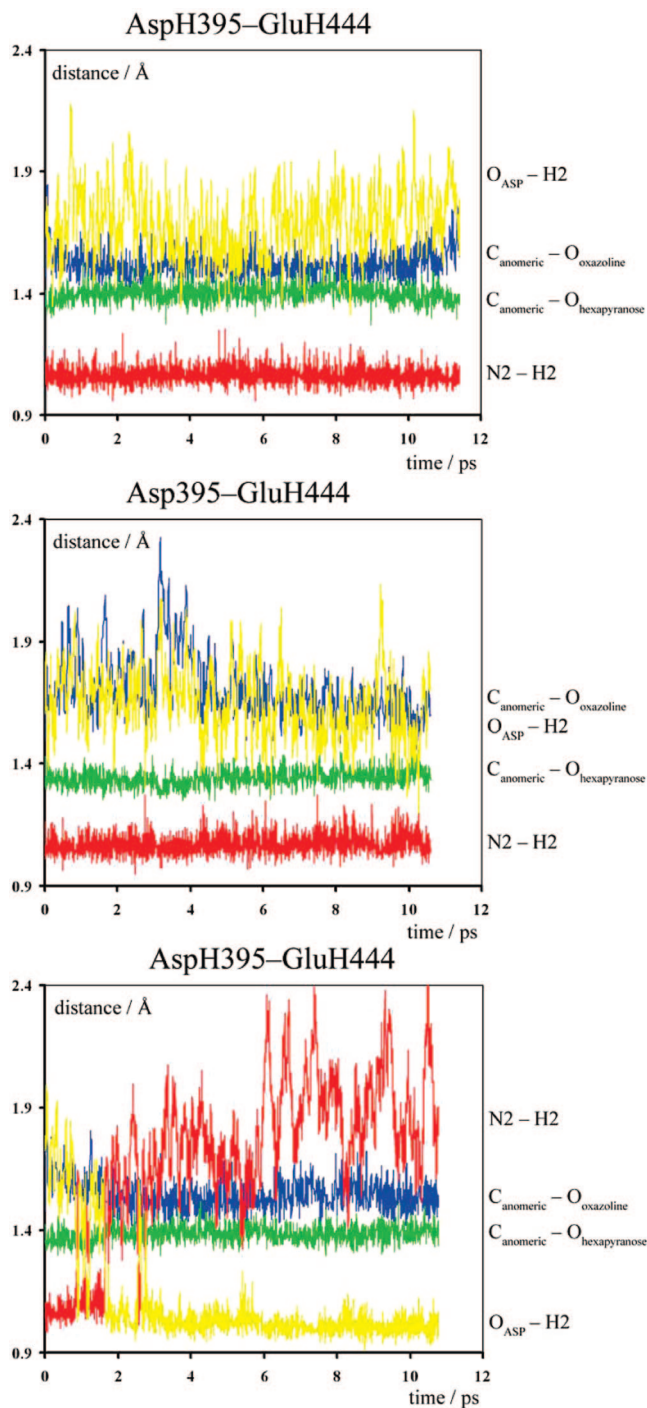(41) Bérces, A.; Whitfield, D. M.; Nukada, T. *Tetrahedron* **2001**, *57*, 477–491.

Figure 7. The evolution of bond distances about the anomeric carbon center and about the oxazolinium nitrogen atom determined during QM/MM simulations of three protonation states of the *Sp*Hex active site.

during the course of all three simulations. During the simulation of AspH395–GluH444, the hydrogen atom (H2) remained localized on the nitrogen atom of the substrate (N2): the average N2–H2 distance observed was 1.07 Å, compared to an O_{Asp}–H2 distance of 1.68 Å. A $C_{anomeric}$–$O_{oxazoline}$ distance of 1.52 Å and a $C_{anomeric}$–$O_{pyranose}$ distance of 1.41 Å were also observed during the course of the simulation. These data are consistent with the presence of an oxazolinium intermediate, electrostatically stabilized by the presence of Asp313 in the active site of *Sp*Hex.

The simulation of Asp395–GluH444 produced markedly different behavior. Although the H2 hydrogen atom remained local-

ized on the substrate's nitrogen atom (average N2–H2 distance = 1.08 Å; average O_{Asp}–H2 distance = 1.64 Å), the $C_{anomeric}$–$O_{oxazoline}$ distance fluctuated around a dramatically increased value of 1.70 Å. Concomitant with this increase in $C_{anomeric}$–$O_{oxazoline}$ distance, a decrease in the $C_{anomeric}$–$O_{pyranose}$ distance to 1.35 Å was observed. These structural characteristics are consistent with the formation of an oxazolinium ion, electrostatically stabilized by Asp313, which is significantly distorted toward a structure associated with an oxacarbenium ion **4**.

The simulation of AspH395–Glu444 again results in different structural behavior. In this simulation, the proton is transferred from N2 to O_{Asp} within the first 2 ps of the simulation and remains localized on that atom for the remainder of the simulation (average N2–H2 distance = 1.82 Å; average O_{Asp}–H2 distance = 1.03 Å). Bonding distances of heteroatoms to the anomeric carbon center are similar to those found in the simulation of AspH395–GluH444, a $C_{anomeric}$–$O_{oxazoline}$ distance of 1.54 Å and a decrease in the $C_{anomeric}$–$O_{pyranose}$ distance to 1.39 Å being observed. These observations are consistent with presence of a neutral enzyme-bound oxazoline intermediate whose formation is catalyzed by the action of Asp313 as a general base. By considering these three simulations together, it is found that longer $C_{anomeric}$–$O_{oxazoline}$ distances are correlated with shorter $C_{anomeric}$–$O_{pyranose}$ distances: this behavior is consistent with expected structural trends arising from the anomeric effect.[43]

Structural differences between each of these three simulations were further characterized by determining the conformation of the pyranose ring at snapshots taken from each trajectory (Figure 8). During the simulation of Asp395–GluH444, the starting $^4C_1$ conformation (from the preparatory MM simulations) was found to rapidly relax to the $^4H_3/^4E/^4H_5$ region of conformational space. The $^4H_3$ and ^4E conformations represent structures in which atoms C2, C1, O5, and C5 are coplanar and the $^4H_5$ conformation is related to the ^4E structure by a small pseudorotational distortion. These conformations are consistent with the variations in bond-length observed at the anomeric center, suggesting significant oxacarbenium ion-like character.

Though the simulations of AspH395–GluH444 and AspH395–Glu444 produced similar distances between the anomeric carbon center and the bonded oxygen atoms, markedly different conformations are observed in each simulation. During the AspH395–Glu444 trajectory, the oxazoline intermediate is found to predominantly occupy the starting $^4C_1$ conformation, though frequent distortions toward oxacarbenium ion-like conformations ($^4H_3/^4E/^4H_5$) are observed. The conformational behavior of AspH395–GluH444 is notable, with rapid relaxation from the $^4C_1$ conformation to the $^1S_3$ conformation being observed. Again a deviation toward the oxacarbenium ion-like ^4E conformation is observed toward the end of the simulation (a slight concomitant increase in the $C_{anomeric}$–$O_{oxazoline}$ bond length also being observed at this time). This apparent correlation between oxazoline protonation state and hexopyranose ring conformation is intriguing. On the basis of crystallographic evidence, it has been proposed that the pyranose conformational itinerary utilized by the GH-18, GH-20, GH-56, and GH-84 families converts the glycoside substrate of the Michaelis complex bound in the $^{1,4}B$ or closely related $^1S_3$

(42) Money, V. A.; Smith, N. L.; Scaffidi, A.; Stick, R. V.; Gilbert, H. J.; Davies, G. J. *Angew. Chem., Int. Ed.* **2006**, *45*, 5136–5140.
(43) Briggs, A. J.; Glenn, R.; Jones, P. G.; Kirby, A. J.; Ramaswamy, P. *J. Am. Chem. Soc.* **1984**, *106*, 6200–6206.
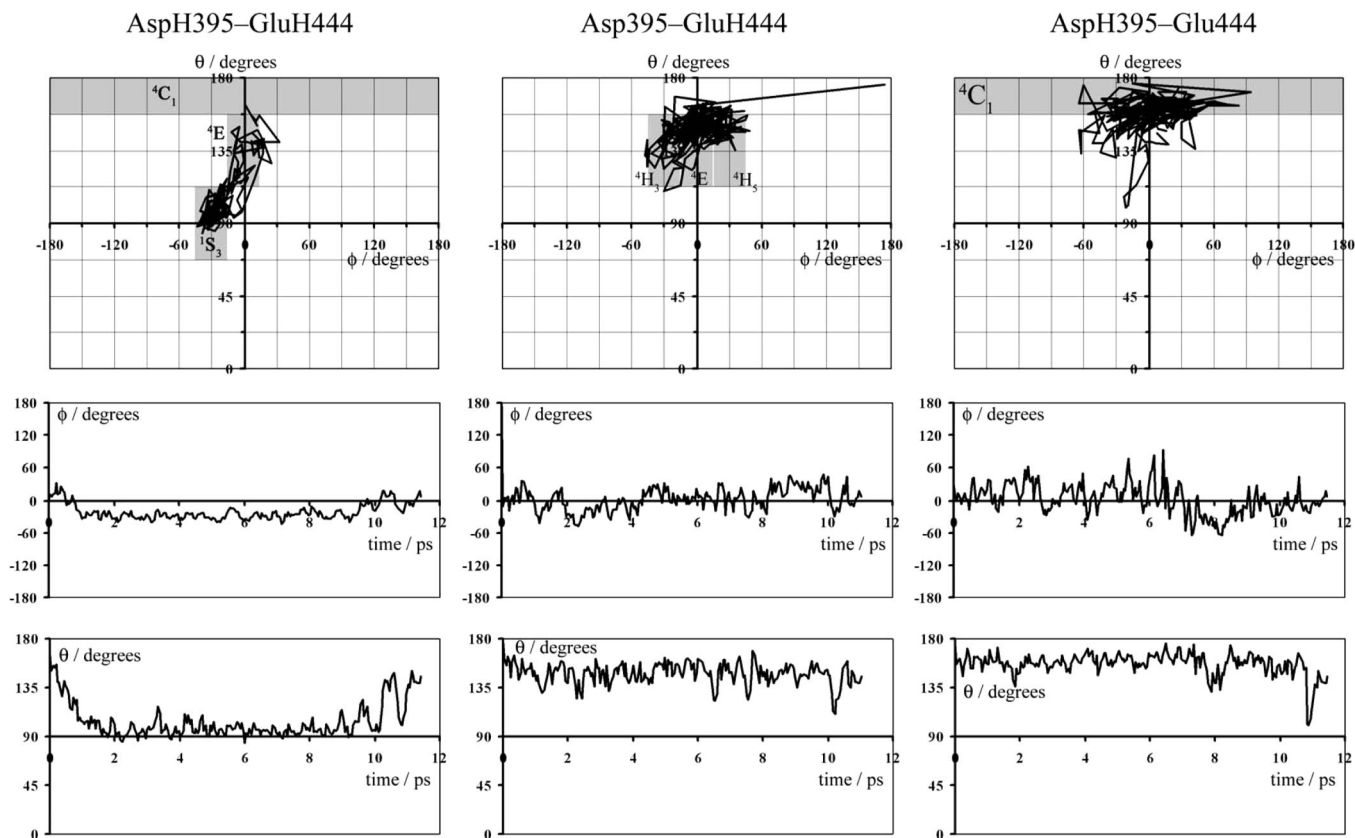
Figure 8. The evolution of hexopyranose ring conformation over the time-course of QM/MM MD simulations of three protonation states of residues within the active site of *Sp*Hex.

conformation[44,45] via a ^{4}E oxacarbenium ion-like transition state (or states)[46] to an oxazoline or oxazolinium ion bound in a flattened ^{4}C$_1$ conformation (Figure 6).[27,47] Current simulations of different protonation states for active site residues predicted to titrate at around the pH-optimum of *Sp*Hex in combination with prior pH-rate studies hint at potentially more complicated conformational behavior.

The ^{4}C$_1$ conformation of the intermediate oxazoline/oxazolinium is inferred from a wealth of crystallographic data in which thiazoline **3** (a nonhydrolyzable transition state or intermediate analogue)[48,49] is bound in the active site. Recent studies of the conformation of thiazoline **3** and derivatives in solution suggest that the observed conformation (as adjudged by vicinal proton coupling constants) is solvent-dependent;[50] further studies show that, in aqueous solutions, the ^3J ^{1}H NMR coupling constants found for the hexopyranose ring of thiazoline **3** are pH-sensitive.[51] While

thiazoline **3** and its *N*-acyl derivatives orient their aliphatic side chains in the hydrophobic binding pocket of GH-84 enzymes in a manner consistent with that found during a reactive pathway,[49] no experimental evidence directly linking the hexopyranose conformation of bound thiazolines **3** to the enzymes' conformational itinerary is available. Furthermore, we expect that the pK_a of the thiazolinium ion of **3** will be significantly lower than that of the associated oxazolinium ion **2** and the predominant protonation state of the enzyme-bound thiazoline need not necessarily match that of the enzyme-bound oxazoline. Detailed NMR-based studies have been used to determine the most prevalent protonation states of glycoside hydrolases in solution.[52−54] The protonation states of titratable active site residues and inhibitors of crystallographically determined glycoside hydrolase structure are however known only in exceptional cases,[55] though predictions may be made on the basis of the distances separating observed heavy atoms. MD simulations play an important role in analyzing alternative likely protonation states.[56] While the protonation state present in the crystal structure might most likely reflects the thermodynamically most favorable protonation state present in the solution from which the crystal was derived, this protonation state need not represent the kinetically

(44) Papanikolau, Y.; Prag, G.; Tavlas, G.; Vorgias, C. E.; Oppenheim, A. B.; Petratos, K. *Biochemistry* **2001**, *40*, 11338–11343.
(45) van Aalten, D. M. F.; Komander, D.; Synstad, B.; Gåseidnes, S.; Peter, M. G.; Eijsink, V. G. H. *Proc. Natl. Acad. Sci. U.S.A.* **2001**, *98*, 8979–8984.
(46) Rao, F. V.; Dorfmueller, H. C.; Villa, F.; Allwood, M.; Eggleston, I. M.; van Aalten, D. M. F. *EMBO J.* **2006**, *25*, 1569–1578.
(47) Dennis, R. J.; Taylor, E. J.; Macauley, M. S.; Stubbs, K. A.; Turkenburg, J. P.; Hart, S. J.; Black, G. N.; Vocadlo, D. J.; Davies, G. J. *Nat. Struct. Mol. Biol.* **2006**, *13*, 365–371.
(48) Knapp, S.; Vocadlo, D. J.; Gao, Z.; Kirk, B.; Lou, J.; Withers, S. G. *J. Am. Chem. Soc.* **1996**, *118*, 6804–6805.
(49) Whitworth, G. E.; Macauley, M. S.; Stubbs, K. A.; Dennis, R. J.; Taylor, E. J.; Davies, G. J.; Greig, I. R.; Vocadlo, D. J. *J. Am. Chem. Soc.* **2007**, *129*, 635–644.
(50) Knapp, S.; Abdo, M.; Ajayi, K.; Huhn, R. A.; Emge, T. J.; Kim, E. J.; Hanover, J. A. *Org. Lett.* **2007**, *9*, 2321–2324.
(51) Macauley, M. S.; Vocadlo, D. J. Personal communication.

(52) Joshi, M. D.; Sidhu, G.; Pot, I.; Brayer, G. D.; Withers, S. G.; McIntosh, L. P. *J. Mol. Biol.* **2000**, *299*, 255–279.
(53) Joshi, M. D.; Sidhu, G.; Nielsen, J. E.; Brayer, G. D.; Withers, S. G.; McIntosh, L. P. *Biochemistry* **2001**, *40*, 10115–10139.
(54) Poon, D. K. Y.; Schubert, M.; Au, J.; Okon, M.; Withers, S. G.; McIntosh, L. P. *J. Am. Chem. Soc.* **2006**, *128*, 15388–15389.
(55) Varrot, A.; Tarling, C. A.; Macdonald, J. M.; Stick, R. V.; Zechel, D. L.; Withers, S. G.; Davies, G. J. *J. Am. Chem. Soc.* **2003**, *125*, 7496–7497.
(56) Mazumder, D.; Kahn, K.; Bruice, T. C. *J. Am. Chem. Soc.* **2002**, *124*, 8825–8833.

significant protonation state.[57] In cases where multiple protonation states likely contribute to the overall rate of reaction, the link between crystallographically determined structure and reactivity is even less secure. [In the case of *Serratia marcescens* Chitinase A, an enzyme belonging to GH-18, an unusual mechanism of glycoside hydrolysis not necessarily involving substrate-assisted catalysis was proposed based on a crystallographic evidence derived from a structure in which the 2-*N*-acetamido group was not appropriately oriented for nucleophilic attack.[44]] A recent analysis of *Thermotoga maritima* GH-1 α-glucosidase inhibition by a series of iminosugar inhibitors (putative transition state analogues) highlights the difficulty in interpreting both crystallographic and thermochemical binding data in terms directly related to glycosidase mechanism.[58]

The findings presented in this paper suggest that a number of quite divergent thermodynamically accessible end-points may exist for the conformational itinerary that is followed by the oxazolinium ion/oxazoline intermediate formed within the active site of *Sp*Hex. All of the structures found lie within the region of conformational space sampled by the crystal structures determined and suggest that the *Sp*Hex-bound intermediate is likely to display a high degree of conformational mobility. This conformational mobility is associated with the unusual nature (at least as far as the GHs are concerned) of the enzyme-bound intermediate formed. The oxazoline possesses a fused 6,5-ring system in which not only the anomeric effect is significant in determining conformation; the tendency toward coplanarity of the C3, C2, C1, and O5 pyranose ring atoms induced by the five-membered ring is also important. The majority of enzymes utilizing the $^{1}S_{3}-^{4}E-^{4}C_{1}$ conformational itinerary (i.e., those not employing anchimeric assistance) form intermediates possessing the $^{4}C_{1}$ conformation: this conformation is expected to be the most thermodynamically stable conformation of a corresponding anomeric α-acylal in solution. As such, these enzymes bind substrates in a distorted conformation but intermediates in an undistorted conformation. Neither $^{4}C_{1}$, ^{4}E, nor $^{1}S_{3}$ conformations however represent the most stable conformation of the oxazoline in solution,[59] and so, the mechanism employed by hexosaminidases utilizing anchimeric assistance may therefore involve a conformational distortion of both substrate and intermediate. Furthermore, it seems likely that the precise electrostatic environment of the enzyme active site plays a role in stabilizing alternative conformations.

The $^{1}S_{3}$ (Michaelis complex)$-^{4}E$ (transition state)$-^{4}C_{1}$ (intermediate) conformational itinerary proposed on the basis of crystallographic studies is consistent with the "antiperiplanar lone pair hypothesis" that is frequently invoked to explain the conformational behavior of glycosides during reactions (particularly those within enzyme active site).[60] Sinnott has shown that, in general, arguments based on the stereoelectronic hypotheses for glycoside hydrolysis are untestable and may best be rationalized in terms of "principle of least nuclear motion" arguments.[61-64] Least motion arguments made in support of particular conformational itineraries associated

with acetal hydrolysis are themselves weakened by the "late" nature of the transition state(s) governing acetal hydrolyses with respect to the bonding patterns found in the product and reactant ground states.[65] Our findings in this regard are consistent with the computational studies of Whitfield et al., which show that "principle of least nuclear motion" and "antiperiplanar lone pair hypothesis" pathways are connected by an almost barrierless pseudorotation pathway.[66]

Conclusions

Oxazolinium ion **2** is predicted to have a pK_a in solution that exceeds that of aspartic acid (in solution), and on this basis, we might predict that the role of Asp313 in the *Sp*Hex active site is to electrostatically stabilize the enzyme-bound intermediate. Relatively high-level QM/MM simulations show however that both the relative pK_a values of oxazolinium ion and Asp313 (reported on by the location of the proton in the Asp313−oxazolinium ion **2** hydrogen bond) and the conformation of the oxazolinium ion itself are sensitive to the protonation states of two peripheral residues within the active site of *Sp*Hex.

Though a complete mechanistic description of alternative hydrolytic pathways examining the influence of different enzymic protonation states at the currently utilized level of theory is beyond the scope of this paper, open questions that should be addressed are clear. Do the theoretically determined mechanisms associated with alternative enzymic protonation states represent kinetically competent pathways (i.e., are our best estimates for computed values of k_{cat} less than or equal to observed values of k_{cat})? Can we accurately compute free energies of binding of substrate to different enzymic protonation states (and hence determine the thermodynamically favorable reaction pathway)? Can structural probes which are sensitive to changes in substrate environment and structure (i.e., kinetic and equilibrium isotope effects) be used in combination with computational models to distinguish among alternative reaction pathways?

While crystallographic data on glycoside hydrolase-bound species seem to conform to both "stereoelectronic control" and "principle of least nuclear motion" rationalizations, it is apparent that further combined kinetic, structural, and theoretical investigations are warranted in the unusual case of hexosaminidases utilizing anchimeric assistance. Simulation of reaction pathways for multiple enzymic protonation states will ultimately allow a critical evaluation of the inferences drawn from a wide variety of experimental sources.

Supporting Information Available: GROMOS96 topology for the MM equilibration of the oxazolinium ion, plot of the controlled deprotonation of oxazolinium ion during QM MD simulations (Figure S1), and abbreviated results of an empirical pK_a prediction performed using the PROPKA software (Table S1). This material is available free of charge via the Internet at http://pubs.acs.org.

JA805640C

(57) Vocadlo, D. J.; Wicki, J.; Rupitz, K.; Withers, S. G. *Biochemistry* **2002**, *41*, 9736–9746.
(58) Gloster, T. M.; Meloncelli, P.; Stick, R. V.; Zechel, D. L.; Vasella, A.; Davies, G. J. *J. Am. Chem. Soc.* **2007**, *129*, 2345–2354.
(59) Foces-Foces, C.; Cano, F. H. *Carbohydr. Res.* **1984**, *135*, 1–11.
(60) Nerinckx, W.; Desmet, T.; Claeyssens, M. *ARKIVOC* **2006**, 90–116.
(61) Sinnott, M. L. *Biochem. J.* **1984**, *224*, 817–821.
(62) Hosie, L.; Marshall, P. J.; Sinnott, M. L. *J. Chem. Soc. Perkin Trans. II* **1984**, 1121–1131.
(63) Bennet, A. J.; Sinnott, M. L. *J. Am. Chem. Soc.* **1986**, *108*, 7287–7294.
(64) Sinnott, M. L. *Adv. Phys. Org. Chem.* **1988**, *24*, 113–204.

(65) Hine, J. *Adv. Phys. Org. Chem.* **1977**, *15*, 1–61.
(66) Ionescu, A. R.; Whitfield, D. M.; Zgierski, M. Z.; Nukada, T. *Carbohydr. Res.* **2006**, *341*, 2912–2920.